Materials Physics and Mechanics 47 (2021) 501-513 Received: June 14, 2021

NONLINEAR DEFORMATION OF BCC METAL Fe AND BCC INTERSTITIAL ALLOY FeSi: DEPENDENCE ON TEMPERATURE, PRESSURE AND SILICON CONCENTRATION

N.Q. Hoc[1], B.D. Tinh[1*], N.D. Hien[2], G. Coman[3]

[1]Hanoi National University of Education, 136 Xuan Thuy, Hanoi, Vietnam

[2]Mac Dinh Chi High School, Chu Pah, Gia Lai, Vietnam

[3]"Dunarea de Jos" University of Galati, Romania

*e-mail: tinhbd@hnue.edu.vn

Abstract. Based on our model and theory of nonlinear deformation for BCC binary interstitial alloy built by the statistical moment method, we perform numerical calculations for characteristic quantities of nonlinear deformation such as the density of deformation energy, the maximum real stress, the limit of elastic deformation together with the stress-strain curve for metal Fe and alloy FeSi with the BCC structure at temperature up to 1100K, pressures up to 10 GPa, and silicon concentrations up to 4%. The calculated results of Fe are compared with experiments and the calculated results of FeSi are our new predictions.
Keywords: nonlinear deformation, interstitial alloy, the density of deformation energy, maximum real stress, limit of elastic deformation, stress-strain curve, statistical moment method

1. Introduction

Iron and its alloys are widely used in structural, electrical, and other technological applications. The dependence of elastic and nonlinear deformations of materials on temperature and pressure has a very important role in order to predict and understand their interatomic interactions, strength, mechanical stability, phase transition mechanisms, and dynamical response.

Iron silicides have paid attention in recent decades due to their unusual physical properties and functional applications [1-10]. β-$FeSi_2$ is a semiconducting phase and has been studied as a material for thermoelectric conversion, solar cells, and optoelectronic applications [1]. Si has been proposed to be a potential light element in the Earth's core based on density, velocity, isotopic and geochemical data [2,3]. In order to assess Si as a constituent of the core, it is necessary to determine the physical properties of the Si-bearing iron phase under extreme conditions. The compressibility of silicides β-$FeSi_2$ and ε-FeSi (B20 structure) at high pressures has been reported [4,5]. The pressure dependence of the structural, optical and elastic properties for β-$FeSi_2$ is described by some works [5,6]. The thermodynamic and elastic properties depending on temperature and pressure of ε-FeSi have also been investigated [7-9]. Iron silicides have also been reported in the field of magnetic application [10].

In [11], silicon does form genuine interstitial compounds when in association with the larger transition-metal atoms of Groups IV and V. Therefore, we proposed a model of interstitial alloy FeSi with the BCC structure in our previous papers [12-21], where in our

http://dx.doi.org/10.18149/MPM.4732021_11

model of interstitial alloy AB with the BCC structure in the concentration condition $c_A << c_B$, the main metal atoms A stay in the vertices and the body center of the cubic unit cell and the interstitial atom B stays in the face centers of the cubic unit cell. In that concentration condition, the interstitial atoms B only stay in the face centers of the cubic unit cell. In our numerical results, $c_B = 0 \div 5\%$. This means that the interstitial atoms B only stay in the face centers of some cubic unit cells and all other cubic unit cells only have the metal atoms A. We have many published papers [12-21], where the main metal atoms A = Fe, W, Ta and the interstitial atoms B = Si, C, H are in the alloys FeSi, FeH, FeC, WSi, TaSi. We still proposed a model of interstitial and substitutional alloy FeCrSi with the BCC structure in our previous papers [22-25], where in our model of interstitial and substitutional alloy ABC with the BCC structure in the concentration condition $c_A << c_B << c_C$, the main metal atoms A stay in the vertices, the substitutional atom B substitutes the main metal atoms A in the body center of the cubic unit cell and the interstitial atom B stays in the face centers of the cubic unit cell. We have some published papers [22-25], where the main metal atoms A = Fe, V, the substitutional atom B = Cr, W, and the interstitial atoms C = Si are in the alloys FeCrSi, VWSi. The above mentioned model of interstitial alloy AB and model of interstitial and substitutional alloy ABC with BCC structure are approximate models for ternary and binary interstitial alloys. Many of our SMM numerical calculations in published papers based on these models are in good agreement with other calculations and data experiments. We have been considered the structural, elastic, thermodynamic, and melting properties of BCC-FeSi in the range of temperature from 0 to 1000K, the range of pressure from 0 to 70 GPa, and the range of interstitial atom from 0 to 5% by the way of SMM in [12,13,15,19]

The experimental data on elastic and nonlinear deformations of iron are presented in [26-28]. The elastic moduli of BCC-Fe under pressure and temperature are studied by the full-potential linear response and linear-muffin-tin orbital generalized gradient approximation (LMTO-GGA) method [29].

In the next section, we present the theory of nonlinear deformation for BCC binary interstitial alloy built by the statistical moment method (SMM) [30-33] and numerical results for metal Fe and alloy FeSi.

2. Content of research

Theory of nonlinear deformation for BCC interstitial alloy AB under pressure. In our model for interstitial alloy AB with BCC structure and concentration condition $c_B << c_A$, the cohesive energy u_0 and the alloy parameters $k, \gamma_1, \gamma_2, \gamma$ (k is called as the harmonic parameter and $\gamma_1, \gamma_2, \gamma$ are called as anharmonic parameters) for the interstitial atom B in face centers of the cubic unit cell, the main metal atom A_1 in body center of the cubic unit cell and the main metal atom A_2 in vertices of the cubic unit cell in the approximation of two coordination spheres have the form [12-25,30-33]

$$u_{0B} = \frac{1}{2}\sum_{i=1}^{n_i}\varphi_{AB}(r_i) = \varphi_{AB}(r_{1B}) + 2\varphi_{AB}(r_{2B}), r_{2B} = \sqrt{2}r_{1B}, \quad (1)$$

$$k_B = \frac{1}{2}\sum_i\left(\frac{\partial^2\varphi_{AB}}{\partial u_{i\beta}^2}\right)_{eq} = \frac{1}{r_{1B}}\frac{d\varphi_{AB}(r_{1B})}{dr_{1B}} + \frac{d^2\varphi_{AB}(r_{2B})}{dr_{2B}^2} + \frac{1}{r_{2B}}\frac{d\varphi_{AB}(r_{2B})}{dr_{2B}}, \quad (2)$$

$$\gamma_B = 4(\gamma_{1B} + \gamma_{2B}), \quad (3)$$

$$\gamma_{1B} = \frac{1}{48}\sum_i\left(\frac{\partial^4\varphi_{AB}}{\partial u_{i\beta}^4}\right)_{eq} = \frac{1}{24}\frac{1}{8r_{1B}^2}\frac{d^2\varphi_{AB}(r_{1B})}{dr_{1B}^2} - \frac{1}{8r_{1B}^3}\frac{d\varphi_{AB}(r_{1B})}{dr_{1B}} + \frac{1}{48}\frac{d^4\varphi_{AB}(r_{2B})}{dr_{2B}^4} +$$

$$+\frac{1}{8r_{2B}}\frac{d^3\varphi_{AB}(r_{2B})}{dr_{2B}^3}-\frac{5}{16r_{2B}^2}\frac{d^2\varphi_{AB}(r_{2B})}{dr_{2B}^2}+\frac{5}{16r_{2B}^3}\frac{d\varphi_{AB}(r_{2B})}{dr_{2B}}, \quad (4)$$

$$\gamma_{2B}=\frac{6}{48}\sum_i\left(\frac{\partial^4\varphi_{AB}}{\partial u_{i\alpha}^2\partial u_{i\beta}^2}\right)_{eq}=\frac{1}{4r_{1B}^2}\frac{d^2\varphi_{AB}(r_{1B})}{dr_{1B}^2}-\frac{1}{4r_{1B}^3}\frac{d\varphi_{AB}(r_{1B})}{dr_{1B}}+\frac{1}{8}\frac{d^4\varphi_{AB}(r_{2B})}{dr_{2B}^4}+$$

$$+\frac{1}{4r_{2B}}\frac{d^3\varphi_{AB}(r_{2B})}{dr_{2B}^3}+\frac{7}{8r_{2B}^2}\frac{d^2\varphi_{AB}(r_{2B})}{dr_{2B}^2}-\frac{7}{8r_{2B}^3}\frac{d\varphi_{AB}(r_{2B})}{dr_{2B}}, \quad (5)$$

$$u_{0A_1}=u_{0A}+\varphi_{AB}\left(r_{1A_1}\right), \quad (6)$$

$$k_{A_1}=k_A+\frac{1}{2}\sum_i\left[\left(\frac{\partial^2\varphi_{AB}}{\partial u_{i\beta}^2}\right)_{eq}\right]_{r=r_{1A_1}}=k_A+\frac{d^2\varphi_{AB}\left(r_{1A_1}\right)}{dr_{1A_1}^2}+\frac{2}{r_{1A_1}}\frac{d\varphi_{AB}\left(r_{1A_1}\right)}{dr_{1A_1}}, \quad (7)$$

$$\gamma_{A_1}=4\left(\gamma_{1A_1}+\gamma_{2A_1}\right), \quad (8)$$

$$\gamma_{1A_1}=\gamma_{1A}+\frac{1}{48}\sum_i\left[\left(\frac{\partial^4\varphi_{AB}}{\partial u_{i\beta}^4}\right)_{eq}\right]_{r=r_{1A_1}}=$$

$$\gamma_{1A}+\frac{1}{24}\frac{d^4\varphi_{AB}(r_{1A_1})}{dr_{1A_1}^4}+\frac{1}{4r_{1A_1}^2}\frac{d^2\varphi_{AB}(r_{1A_1})}{dr_{1A_1}^2}-\frac{1}{4r_{1A_1}^3}\frac{d\varphi_{AB}(r_{1A_1})}{dr_{1A_1}}, \quad (9)$$

$$\gamma_{2A_1}=\gamma_{2A}+\frac{6}{48}\sum_i\left[\left(\frac{\partial^4\varphi_{AB}}{\partial u_{i\alpha}^2\partial u_{i\beta}^2}\right)_{eq}\right]_{r=r_{1A_1}}=$$

$$\gamma_{2A}+\frac{1}{2r_{1A_1}}\frac{d^3\varphi_{AB}(r_{1A_1})}{dr_{1A_1}^3}-\frac{3}{4r_{1A_1}^2}\frac{d^2\varphi_{AB}(r_{1A_1})}{dr_{1A_1}^2}+\frac{3}{4r_{1A_1}^3}\frac{d\varphi_{AB}(r_{1A_1})}{dr_{1A_1}}, \quad (10)$$

$$u_{0A_2}=u_{0A}+\varphi_{AB}\left(r_{1A_2}\right), \quad (11)$$

$$k_{A_2}=k_A+\frac{1}{2}\sum_i\left[\left(\frac{\partial^2\varphi_{AB}}{\partial u_{i\beta}^2}\right)_{eq}\right]_{r=r_{1A_2}}=k_A+2\frac{d^2\varphi_{AB}\left(r_{1A_2}\right)}{dr_{1A_2}^2}+\frac{4}{r_{1A_2}}\frac{d\varphi_{AB}\left(r_{1A_2}\right)}{dr_{1A_2}}, \quad (12)$$

$$\gamma_{A_2}=4\left(\gamma_{1A_2}+\gamma_{2A_2}\right), \quad (13)$$

$$\gamma_{1A_2}=\gamma_{1A}+\frac{1}{48}\sum_i\left[\left(\frac{\partial^4\varphi_{AB}}{\partial u_{i\beta}^4}\right)_{eq}\right]_{r=r_{1A_2}}=\gamma_{1A}+\frac{1}{24}\frac{d^4\varphi_{AB}(r_{1A_2})}{dr_{1A_2}^4}+\frac{1}{4r_{1A_2}}\frac{d^3\varphi_{AB}(r_{1A_2})}{dr_{1A_2}^3}-$$

$$-\frac{1}{8r_{1A_2}^2}\frac{d^2\varphi_{AB}(r_{1A_2})}{dr_{1A_2}^2}+\frac{1}{8r_{1A_2}^3}\frac{d\varphi_{AB}(r_{1A_2})}{dr_{1A_2}}, \quad (14)$$

$$\gamma_{2A_2}=\gamma_{2A}+\frac{6}{48}\sum_i\left[\left(\frac{\partial^4\varphi_{AB}}{\partial u_{i\alpha}^2\partial u_{i\beta}^2}\right)_{eq}\right]_{r=r_{1A_2}}=\gamma_{2A}+\frac{1}{4}\frac{d^4\varphi_{AB}(r_{1A_2})}{dr_{1A_2}^4}-$$

$$-\frac{1}{4r_{1A_2}}\frac{d^3\varphi_{AB}(r_{1A_2})}{dr_{1A_2}^3}+\frac{3}{2r_{1A_2}^2}\frac{d^2\varphi_{AB}(r_{1A_2})}{dr_{1A_2}^2}-\frac{3}{2r_{1A_2}^3}\frac{d\varphi_{AB}(r_{1A_2})}{dr_{1A_2}}, \quad (15)$$

where φ_{AB} is the interaction potential between atoms A and B, $r_{1X} = r_{01X} + y_{0X}(T)$ is the nearest neighbor distance between the atom X (X = A, A_1, A_2, B) (A in clean metal, A_1, A_2, and B in interstitial alloy AB) and other atoms at temperature T, r_{01X} is the nearest neighbor distance between the atom X and other atoms at T = 0K and is determined from the minimum condition of the cohesive energy $u_{0X}, y_{0X}(T)$ is the displacement of atom X from equilibrium position at temperature T. $u_{0A}, k_A, \gamma_{1A}, \gamma_{2A}$ is the corresponding quantities in the clean metal A with BCC structure in the approximation of two coordination spheres [12-25,30-33]

$$u_{0A} = 4\varphi_{AA}(r_{1A}) + 3\varphi_{AA}(r_{2A}),\ r_{2A} = \frac{2}{\sqrt{3}} r_{1A}, \tag{16}$$

$$k_A = \frac{4}{3}\frac{d^2\varphi_{AA}(r_{1A})}{dr_{1A}^2} + \frac{8}{3r_{1A}}\frac{d\varphi_{AA}(r_{1A})}{dr_{1A}} + \frac{d^2\varphi_{AA}(r_{2A})}{dr_{2A}^2} + \frac{2}{r_{2A}}\frac{d\varphi_{AA}(r_{2A})}{dr_{2A}}, \tag{17}$$

$$\gamma_{1A} = \frac{1}{54}\frac{d^4\varphi_{AA}(r_{1A})}{dr_{1A}^4} + \frac{8}{9r_{1A}}\frac{d^3\varphi_{AA}(r_{1A})}{dr_{1A}^3} - \frac{20}{9r_{1A}^2}\frac{d^2\varphi_{AA}(r_{1A})}{dr_{1A}^2} + \frac{20}{9r_{1A}^3}\frac{d\varphi_{AA}(r_{1A})}{dr_{1A}} + \frac{1}{24}\frac{d^4\varphi_{AA}(r_{2A})}{dr_{2A}^4} + \frac{1}{4r_{2A}^2}\frac{d^2\varphi_{AA}(r_{2A})}{dr_{2A}^2} - \frac{1}{4r_{2A}^3}\frac{d\varphi_{AA}(r_{2A})}{dr_{2A}}, \tag{18}$$

$$\gamma_{2A} = \frac{1}{54}\frac{d^4\varphi_{AA}(r_{1A})}{dr_{1A}^4} + \frac{5}{9r_{1A}}\frac{d^3\varphi_{AA}(r_{1A})}{dr_{1A}^3} + \frac{5}{18r_{1A}^2}\frac{d^2\varphi_{AA}(r_{1A})}{dr_{1A}^2} - \frac{5}{18r_{1A}^3}\frac{d\varphi_{AA}(r_{1A})}{dr_{1A}} + \frac{1}{2r_{2A}}\frac{d^3\varphi_{AA}(r_{2A})}{dr_{2A}^3} - \frac{9}{8r_{2A}^2}\frac{d^2\varphi_{AA}(r_{2A})}{dr_{2A}^2} + \frac{9}{8r_{2A}^3}\frac{d\varphi_{AA}(r_{2A})}{dr_{2A}}. \tag{19}$$

The equations of state for BCC interstitial alloy at temperature T and pressure P and at 0K and pressure P are written in the form [12,13,15-21,23,24,30-33]

$$Pv = -r_1\left(\frac{1}{6}\frac{\partial u_0}{\partial r_1} + \theta x c t h x \frac{1}{2k}\frac{\partial k}{\partial r_1}\right),\ v = \frac{4r_1^3}{3\sqrt{3}}. \tag{20}$$

$$Pv = -r_1\left(\frac{1}{6}\frac{\partial u_0}{\partial r_1} + \frac{\hbar\omega_0}{4k}\frac{\partial k}{\partial r_1}\right). \tag{21}$$

From that, we can calculate the nearest neighbor distance $r_{1X}(P,0)(X = A, A_1, A_2, B)$, the parameters $k_X(P,0), \gamma_{1X}(P,0), \gamma_{2X}(P,0), \gamma_X(P,0)$, the displacement $y_{0X}(P,T)$ of atom X from equilibrium position as in [29], the nearest neighbor distance $r_{1X}(P,T)$, and the mean nearest neighbor distance between two atoms in the alloy $\overline{r_{1A}(P,T)}$ as follows[12,13,15-21,23,24,30-33]

$$\begin{aligned}
&r_{1B}(P,T) = r_{1B}(P,0) + y_{A_1}(P,T),\ r_{1A}(P,T) = r_{1A}(P,0) + y_A(P,T),\\
&r_{1A_1}(P,T) \approx r_{1B}(P,T),\ r_{1A_2}(P,T) = r_{1A_2}(P,0) + y_B(P,T).
\end{aligned} \tag{22}$$

$$\begin{aligned}
&\overline{r_{1A}(P,T)} = \overline{r_{1A}(P,0)} + \overline{y(P,T)},\\
&\overline{r_{1A}(P,0)} = (1-c_B)r_{1A}(P,0) + c_B r'_{1A}(P,0),\ r'_{1A}(P,0) = \sqrt{3}r_{1B}(P,0),\\
&\overline{y(P,T)} = (1-7c_B)y_A(P,T) + c_B y_B(P,T) + 2c_B y_{A_1}(P,T) + 4c_B y_{A_2}(P,T).
\end{aligned} \tag{23}$$

The Helmholtz free energy of BCC interstitial alloy AB with the condition $c_B << c_A$ is determined by[12-25,30-33]

$$\psi_{AB} = (1-7c_B)\psi_A + c_B\psi_B + 2c_B\psi_{A_1} + 4c_B\psi_{A_2} - TS_c,$$

$$\psi_X \approx U_{0X} + \psi_{0X} + 3N\left\{\frac{\theta^2}{(k_X)^2}\left[\gamma_{2X}(Y_X)^2 - \frac{2\gamma_{1X}}{3}\left(1+\frac{Y_X}{2}\right)\right] + \right.$$
$$\left. + \frac{2\theta^3}{(k_X)^4}\left[\frac{4}{3}\gamma_{2X}Y_X\left(1+\frac{Y_X}{2}\right) - 2\left[(\gamma_{1X})^2 + 2\gamma_{1X}\gamma_{2X}\left[1+\frac{Y_X}{2}\right](1+Y_X)\right]\right]\right\},$$
$$\psi_{0X} = 3N\theta\left[x_X + \ln\left(1-e^{-2x_X}\right)\right], Y_X \equiv x_X \coth x_X, \quad (24)$$

where ψ_X is the Helmholtz free energy of one atom X, U_{0X} is the cohesive energy, and S_c is the configurational entropy of BCC interstitial alloy AB.

The nearest neighbor distances between two atoms in alloy after deformation $r_{1X}^F(P,0), r_{1X}^F(P,T)$ in alloy have the form

$$r_{1X}^F(P,0) = r_{1X}(P,0)(1+\varepsilon), \quad (25)$$

$$r_{1X}^F(P,T) = r_{1X}(P,T) + \varepsilon . r_{1X}(P,0)(2+\varepsilon). \quad (26)$$

The relationship between the stress and the deformation in nonlinear deformation is given by

$$\sigma_{lAB} = \sigma_{oAB}\frac{\varepsilon_F^{\alpha_{AB}}}{1+\varepsilon_F}, \quad (27)$$

where σ_{oAB} and α_{AB} are constants for every interstitial alloy.

The density of deformation energy can be written in the form

$$f_{AB}(\varepsilon) = \frac{1}{N}(1-7c_B)\left\{\Psi_A\left(\frac{1}{v_{AB}^F}-\frac{1}{v_{AB}}\right) + \frac{2\varepsilon r_{01A}^F}{v_{AB}^F}\left(\frac{\partial\Psi_A^F}{\partial r_{1A}^F}\right)_T + \frac{\varepsilon^2}{2v_{AB}^F}\left[\left(\frac{\partial^2\Psi_A^F}{\partial r_{1A}^{F2}}\right)_T\left(2r_{01A}^F\right)^2 + \left(\frac{\partial\Psi_A^F}{\partial r_{1A}^F}\right)_T 2r_{01A}\right.\right.$$
$$+\frac{c_B}{N}\left\{\Psi_B\left(\frac{1}{v_{AB}^F}-\frac{1}{v_{AB}}\right) + \frac{2\varepsilon r_{01B}^F}{v_{AB}^F}\left(\frac{\partial\Psi_B^F}{\partial r_{1B}^F}\right)_T + \frac{\varepsilon^2}{2v_{AB}^F}\left[\left(\frac{\partial^2\Psi_B^F}{\partial r_{1B}^{F2}}\right)_T\left(2r_{01B}^F\right)^2 + \left(\frac{\partial\Psi_B^F}{\partial r_{1B}^F}\right)_T 2r_{01B}\right]\right\} +$$
$$+\frac{2c_B}{N}\left\{\Psi_{A_1}\left(\frac{1}{v_{AB}^F}-\frac{1}{v_{AB}}\right) + \frac{2\varepsilon r_{01A_1}^F}{v_{AB}^F}\left(\frac{\partial\Psi_{A_1}^F}{\partial r_{1A_1}^F}\right)_T + \frac{\varepsilon^2}{2v_{AB}^F}\left[\left(\frac{\partial^2\Psi_{A_1}^F}{\partial r_{1A_1}^{F2}}\right)_T\left(2r_{01A_1}^F\right)^2 + \left(\frac{\partial\Psi_{A_1}^F}{\partial r_{1A_1}^F}\right)_T 2r_{01A_1}\right]\right\} +$$
$$\left.+\frac{4c_B}{N}\left\{\Psi_{A_2}\left(\frac{1}{v_{AB}^F}-\frac{1}{v_{AB}}\right) + \frac{2\varepsilon r_{01A_2}^F}{v_{AB}^F}\left(\frac{\partial\Psi_{A_2}^F}{\partial r_{1A_2}^F}\right)_T + \frac{\varepsilon^2}{2v_{AB}^F}\left[\left(\frac{\partial^2\Psi_{A_2}^F}{\partial r_{1A_2}^{F2}}\right)_T\left(2r_{01A_2}^F\right)^2 + \left(\frac{\partial\Psi_{A_2}^F}{\partial r_{1A_2}^F}\right)_T 2r_{01A_2}\right]\right\}. \quad (28)$$

When the deformation rate is constant, the density of deformation energy of alloy is determined by

$$f_{AB}(\varepsilon) = C_{AB}.\sigma_{AB}.\varepsilon, \quad (29)$$

where C_{AB} is the proportional factor. At the maximum value of the density of deformation energy, we have

$$f_{AB}\left(\varepsilon_{AB}^F\right) = f_{ABmax} = C_{AB}\sigma_{ABmax}\varepsilon_{AB}^F. \quad (30)$$

The maximum value of stress σ_{ABmax} and the maximum real stress σ_{1ABmax} are

$$\sigma_{ABmax} = \frac{f_{ABmax}}{C_{AB}\varepsilon_{AB}^F},\ \sigma_{1ABmax} = \frac{\sigma_{ABmax}}{1+\varepsilon_{AB}^F} = \frac{f_{ABmax}}{C_{AB}\varepsilon_{AB}^F(1+\varepsilon_{AB}^F)}. \quad (31)$$

From the maximum condition of stress $\left(\frac{\partial\sigma_{ABl}}{\partial\varepsilon}\right)_{\varepsilon_{AB}^F} = 0,$ we derive the deformation ε_{AB}^F corresponding to the maximum value of real stress as follows

$$\varepsilon_{AB}^{F} = \frac{\alpha_{AB}}{1-\alpha_{AB}},\ \sigma_{lABmax} = \sigma_{0AB}\frac{\left(\varepsilon_{AB}^{F}\right)^{\alpha_{AB}}}{1+\varepsilon_{AB}^{F}}. \tag{32}$$

C_{AB} is determined from the experimental condition of stress $\sigma_{0.2AB}$ in the alloy in the form

$$C_{AB} = \frac{f_{AB}(\varepsilon_{0.2AB})}{\sigma_{0.2AB}\varepsilon_{0.2AB}}. \tag{33}$$

From the obtained value of ε_{AB}^{F} we can calculate σ_{0AB} and α_{AB}. The limit of elastic deformation of interstitial alloy AB is determined by

$$E_{AB}\varepsilon_e = \sigma_{0AB}\frac{\varepsilon_{ABe}^{\alpha_{AB}}}{1+\varepsilon_{Ae}}. \tag{34}$$

Numerical results for alloy FeSi. To describe the interaction between atoms Fe and Si, we apply the Mie-Lennard-Jones pair interaction potential in the form [34]

$$\varphi(r) = \frac{D}{n-m}\left[m\left(\frac{r_0}{r}\right)^{n} - n\left(\frac{r_0}{r}\right)^{m}\right], \tag{35}$$

where D is the depth of potential well corresponding to the equilibrium distance r_0, m and n are determined empirically. Then, the potential parameters for the interaction Fe-Si are determined by [35]

$$D_{Fe-Si} = \sqrt{D_{Fe-Fe}D_{Si-Si}},\ r_{0Fe-Si} = \frac{1}{2}\left(r_{0Fe-Fe} + r_{0Si-Si}\right). \tag{36}$$

We find $m_{Fe\text{-}Si}$ and $n_{Fe\text{-}Si}$ by fitting the theoretical result with the experimental data for the Young modulus of interstitial alloy $FeSi_{3\%}$ at room temperature. The Mie-Lennard-Jones potential parameters for the interactions Fe-Fe, Si-Si, and Fe-Si are given in Table 1. The Poisson ratio of Fe is 0.29 [36].

Table 1. Mie-Lennard-Jones potential parameters for interactions Fe-Fe, Si-Si and Fe-Si

Interaction	D (eV)	r_0 (10^{-10} m)	m	n
Fe-Fe [34]	0.401	2.4775	7	11.5
Si-Si [35]	2.32	2.351	2.48	4.0
Fe-Si (proposal)	0.965	2.4142	2.4	5.2

Our calculations for FeSi and Fe are shown in tables from Table 2 to Table 5 and figures from Fig. 1 to Fig. 7.

Table 2. The maximum value of real stress σ_{1max} and the limit of elastic deformation σ_e for FeSi alloys at P = 0 and T = 300K calculated by SMM

c_{Si}(%)	σ_{1max} (MPa)	ε_F (%)	σ_e (MPa)	ε_e (%)
1	243.10	6.6	200.31	0.11
2	250.46	6.8	206.53	0.12
3	258.70	7.0	213.56	0.14
4	279.37	7.0	233.30	0.16
5	296.44	7.0	250.28	0.19

Table 3. The limit of elastic deformation σ_e and the maximum value of real stress σ_{1max} for $FeSi_{2\%}$ at different pressures and T = 300K

P (GPa)	c_{Si}(%)	σ_{1max} (MPa)	ε_F(%)	σ_e (MPa)	ε_e (%)
4	0	247.43	6.5	203.17	0.09
	2	243.34	7.0	197.98	0.11
	4	268.57	7.1	221.83	0.14
10	0	251.43	6.9	201.70	0.08
	2	237.78	7.4	188.19	0.09
	4	250.09	7.6	199.40	0.11

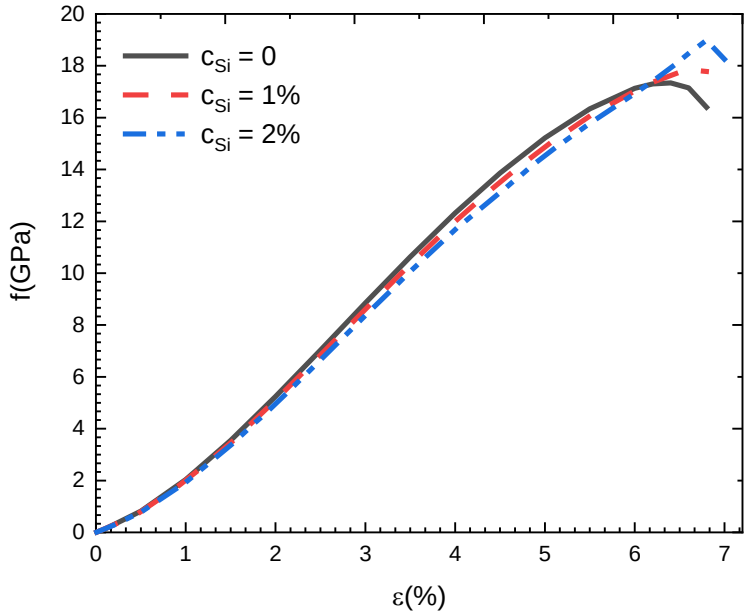

Fig. 1. The density of deformation energy f(ε) for FeSi at different strains, T = 300K and P = 0 calculated by SMM

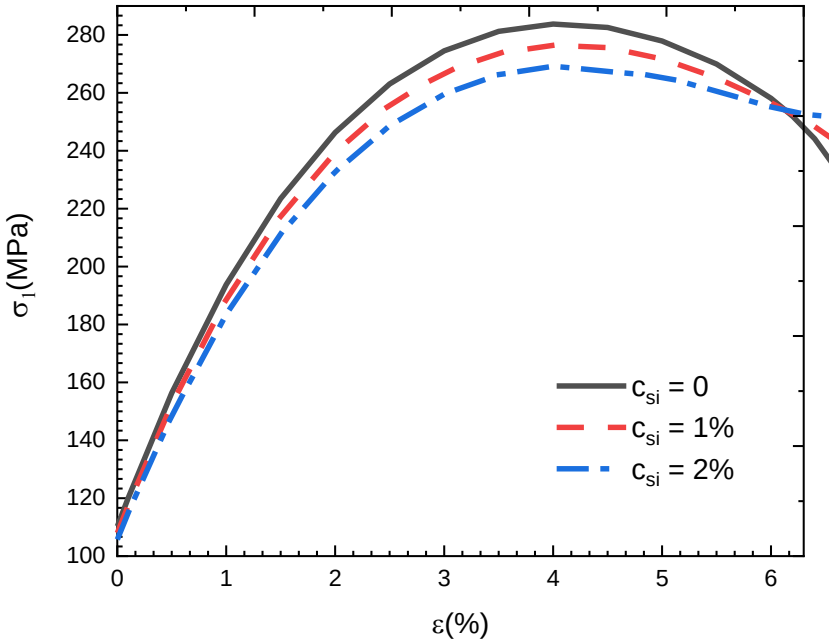

Fig. 2. The real stress $\sigma_1(\varepsilon)$ for FeSi at different silicon concentration and strains, T = 300K and P = 0 calculated by SMM

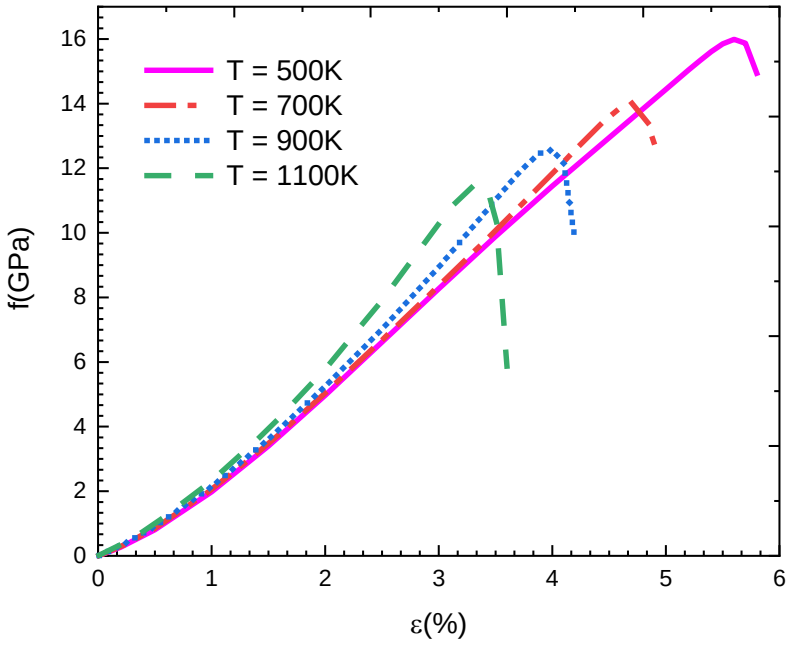

Fig. 3. The density of deformation energy f(ε) for FeSi at different temperatures and strains, c_{Si} = 2% and P = 0 calculated by SMM

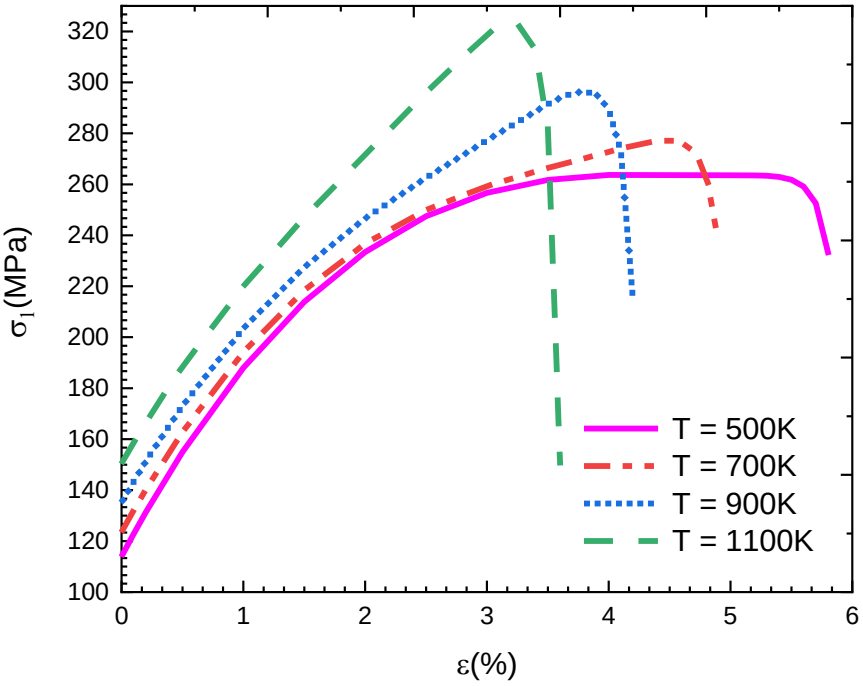

Fig. 4. The real stress $\sigma_1(\varepsilon)$ for FeSi at different temperatures and strains, c_{Si} = 2% and P = 0 calculated by SMM

Figure 5 shows the stress-strain relationship of alloys $FeSi_{1\%}$ at P = 0 and different temperatures from the SMM calculations. When $\varepsilon > 0.5\%$ the alloy FeSi is in the stage of nonlinear deformation and the $\sigma - \varepsilon$ dependence is described in the form of a complex curve. The stage of nonlinear deformation is an irreversible process. In the limit case, our obtained stress-strain curve of metal Fe is in relatively good agreement with the experimental curve of Singh et al. (2007) [26]. At a fixed strain ε, the stress σ decreases when the concentration of

interstitial atoms increases. Adding silicon to iron to formulate steel will increase the strength and the hardness but will decrease the plasticity and toughness.

Our calculations for nonlinear deformation of clean metal Fe are shown in Table 4, Table 5, and Fig. 7. Table 4 shows the dependence of the density of deformation energy $f(\varepsilon)$ and the maximum value of the real stress of Fe on the deformation ε. The graph $f(\varepsilon)$ exists one maximum point (ε_F, f_{max}). When the temperature increases, both ε_p and f_{max} decreases. Knowing ε_F and f_{max}, we can determine the maximum value of real stress σ_{1max} when happens nonlinear deformation.

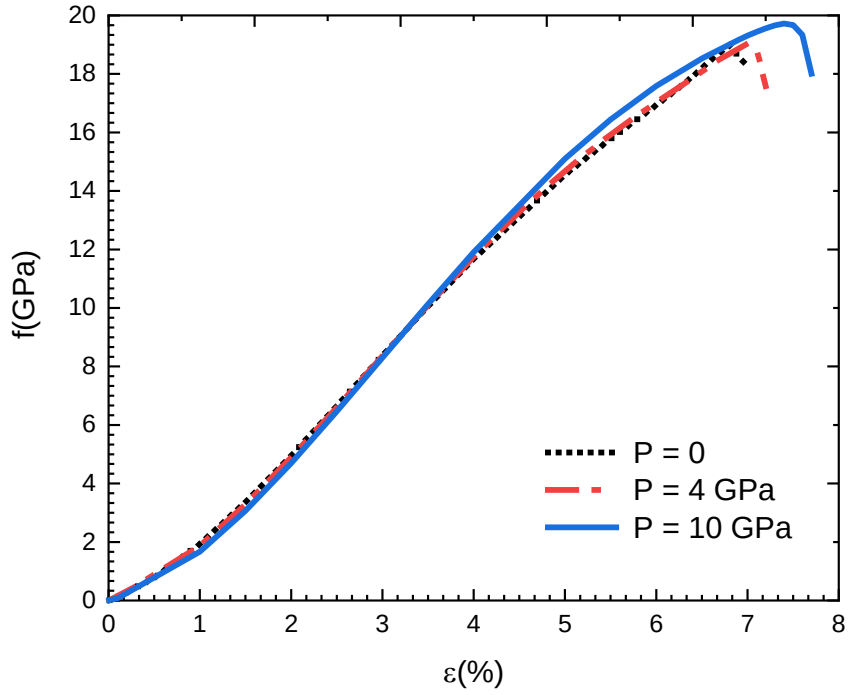

Fig. 5. The density of deformation energy f(ε) for FeSi at different pressure and strains, c_{Si} = 2% and T = 300K calculated by SMM

Table 4. The dependence of the density of deformation energy $f(\varepsilon)$ (GPa) and the real stress σ_1 (MPa) on strain ε (%) for Fe at T = 300K and P = 0 calculated by SMM

ε	1	2	3	4	5	6	6.2	6.4	6.6
$f(\varepsilon)$	2.04	5.24	8.85	12.32	15.22	17.13	17.30	17.34	17.15
σ_{1max}	193.79	246.31	274.53	283.78	277.93	258.12	251.86	244.12	233.67

Table 5 compares the SMM results and the experimental data for the maximum value of real stress and the limit of elastic deformation for Fe at P = 0 and room temperature.

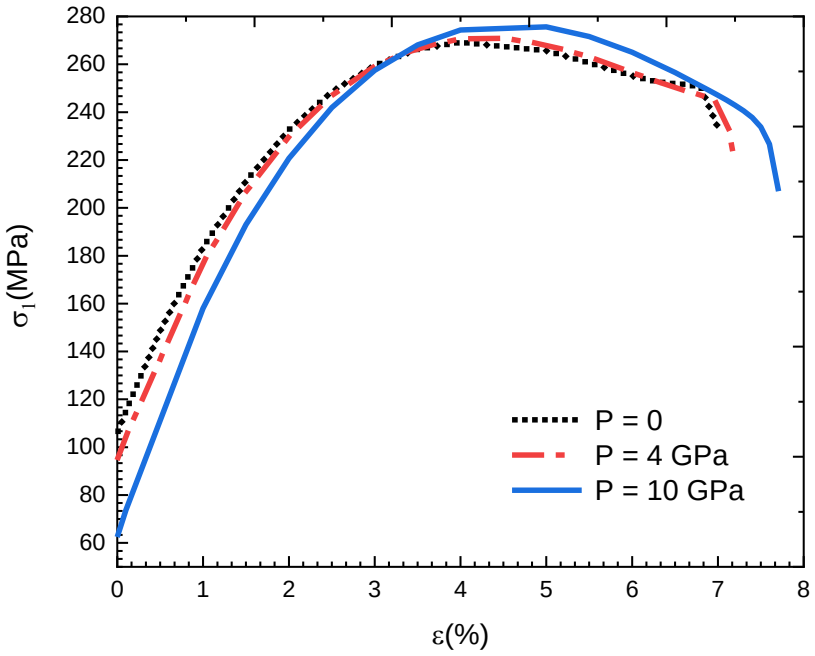

Fig. 6. The real stress $\sigma_1(\varepsilon)$ for FeSi at different pressures and strains, c_{Si} = 2% and T = 300K calculated by SMM

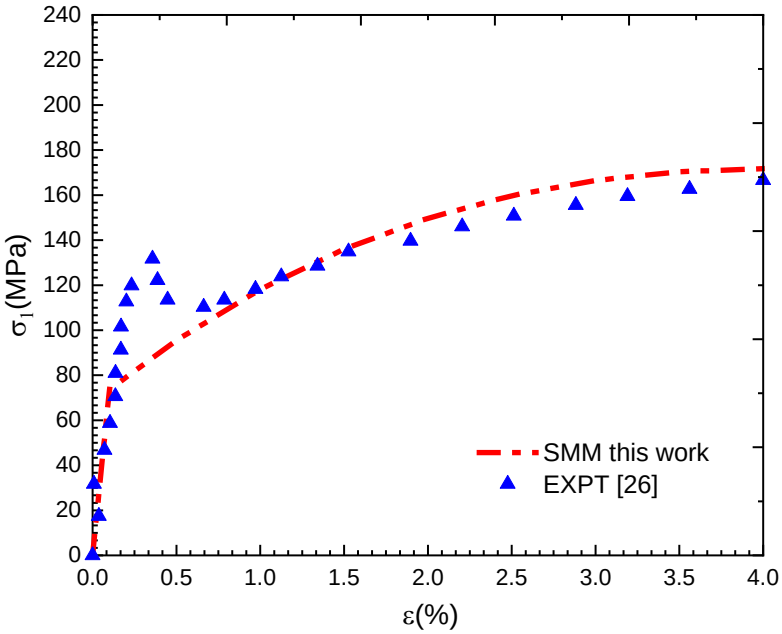

Fig. 7. The real stress σ_1 for Fe at different strains, T = 323 K and P = 0 calculated by SMM (choose experimental stress $\sigma_{0.2}$ = 79 MPa [26]) and from EXPT [26]

Table 5. The maximum value of real stress σ_{1max} and the limit of elastic deformation σ_e for Fe at P = 0 and T = 300K calculated by SMM and from experiments [26,37,38]

	σ_{1max} (MPa)	σ_e (MPa)
SMM this work	244	201
EXPT [26]	240	180
EXPT [37]	296	204
EXPT [38]	230 - 345	110 - 220

3. Conclusions

From the obtained theoretical results and using the combination of the Mie-Lennard-Jones potential and our proposed potential or the Mie-Lennard-Jones potential, we calculated numerically characteristic quantities for nonlinear deformation of BCC-FeSi. We obtain the values of density of deformation energy, maximum real stress, the limit of elastic deformation, and the stress-strain curve and compare the calculated results with experiments for Fe. Some of our calculated results for Fe are in good agreement with available experiments and other calculated results predict experiments in the future.

Acknowledgements. *No external funding was received for this study.*

References

[1] Maeda Y. Semiconducting β-FeSi2 towards optoelectronics and photonics. *Thin Solid Films.* 2007;515: 8118-8121.

[2] Brosh E, Makov G, Shneck RZ. Application of CALPHAD to high pressures. *Calphad.* 2007;31: 173-185.

[3] Georg RB, Halliday AN, Schauble EA, Reynolds BC. Silicon in the Earth's core. *Nature.* 2007;447: 1102-1106.

[4] Santamaria-Pérez D, Nuss J, Haines J, Jansen M, Vegas A. Iron Silicides and Their Corresponding Oxides: A High-Pressure Study of Fe_5Si_3. *Solid State Science.* 2004;6: 673-678.

[5] IchiTani J, Takahashi M, Kido H. Lattice dynamics of β-$FeSi_2$ from first-principles calculations. *Physica B: Condensed Matter.* 2010;405: 2200-2204.

[6] Takarabe TK, Teranishi R, Oinuma J, Mori Y, Udono H, Kikuma I. Structural study of $FeSi_2$ under pressure. *Journal of Applied Physíc.* 2004;96: 4903-4908.

[7] Whitaker MI, Wei I, Qiong I, Liping W, Baosheng I. Thermoelasticity of ε-FeSi to 8 GPa and 1273 K. *American Mineralogy*. 2009;94: 1039-1044.

[8] Whitaker MI, Liu W, Liu Q, Wang I, Li B. Combined in situ synchrotron X-ray diffraction and ultrasonic interferometry study of ϵ-FeSi at high pressure. *High Pressure Research.* 2008;28(3): 385-395.

[9] Petrova AE, Krasnorussky VN, Stishov SM. Elastic properties of FeSi. *Journal of Experimental and Theoretical Physics*. 2010;111: 427–430.

[10] Guan J, Chen X, Zhang L, Wang J, Liang C. Rapid preparation and magnetic properties of Fe_3Si–Al_2O_3 nanocomposite by mechanical alloying and heat treatment. *Physica Status Solidi A.* 2016;213(6): 1585-1591

[11] Goldschmidt HJ. *Interstitial alloys*. Boston, MA: Springer; 1967.

[12] Hoc NQ, Viet LH. Influence of vacancy on thermodynamic properties of interstitial alloy FeSi with BCC structure under pressure. In: *Proc. of the 10th National Conference on Solid State Physics and Material Science* (*SPMS*). 2017. p.907-910.

[13] Hoc NQ, Hien ND. Study on elastic deformation of interstitial alloy AB with BCC structure under pressure. In: *Proc. of the 10th National Conference on Solid State Physics and Material Science* (*SPMS*). 2017. p.911-914.

[14] Tinh BD, Hoc NQ, Vinh DQ, Cuong TD, Hien ND. Thermodynamic and Elastic Properties of Interstitial Alloy FeC with BCC Structure at Zero Pressure. *Advances in Materials Science and Engineering.* 2018; 5251741.

[15] Hoc NQ, Hoa NT, Hien ND, Thang DQ. Study on nonlinear deformation of binary interstitial alloy AB with BCC structure under pressure. *HNUE Journal of Science, Natural Sciences.* 2018;63(6): 57-65.

[16] Hoc NQ, Tinh BD, Cuong TD, Viet LH. Study on the Melting of the Defective Interstitial Alloys TaSi and WSi with BCC Structure. *Journal of the Korean Physical Society,* 2019;74(8): 801-805.
[17] Tuyen LTC, Hoc NQ, Tinh BD, Cuong TD, Vinh DQ. Study on the melting of interstitial alloys FeH and FeC with BCC structure under pressure. *Chinese Journal of Physics.* 2019;59: 1-9.
[18] Hoc NQ, Cuong TD, Hien ND. Study on Elastic Deformation of Interstitial Alloy FeC with BCC Structure under Pressure. *Journal of Sciences: Mathematics-Physics.* 2019;35(1): 1-12.
[19] Hoc NQ, Hoa NT, Cuong TD, Thang DQ. On the melting of interstitial alloys FeH, FeSi and FeC with a body-centred cubic structure under pressure. *Vietnam Journal of Science, Technology and Engineering.* 2018;61(2): 17-22.
[20] Hoa NT, Hoc NQ, Coman G, Vinh DQ, Cuong TD. Thermodynamic properties of BCC interstitial alloy FeH under pressure. *IOP Conference Series: Materials Science and Engineering.* 2018;485: 012017.
[21] Hoc NQ, Hien ND, Van CL, Dung NT, Ţălu S. Study on the Melting Temperature, the Jumps of Volume, Enthalpy and Entropy at Melting Point, and the Debye Temperature for the BCC Defective and Perfect Interstitial Alloy WSi under Pressure. *Journal of Composites Science.* 2021;5(6): 153.
[22] Hoc NQ, Hanh PTM, Huong DT, Ngoc DB, Huyen TT, Viet LH. Influence of vacancy on thermal expansion coefficient and heat capacity at constant pressure of interstitial alloy FeCrSi with BCC structure at zero pressure. *Journal of Military Science and Technology.* 2018;54A: 68-77.
[23] Hoc NQ, Hien ND. Study on elastic deformation of substitution alloy AB with interstitial atom C and BCC structure under pressure.*IOP Conf. Series: Journal of Physics: Conf. Series.* 2018;1034: 012005.
[24] Hoc NQ, Vinh DQ, Hong LP, Loan PTT, Anh NQ, Linh HT. Research on melting theory of substitutional alloys AB interspersed with C atom with BCC structure. *Journal of Science of HNUE, Natural Sciences.* 2017;62(2): 17-26.
[25] Hoc NQ, Viet LH, Anh NNL, Ngoc NB. Effect of vacancy on thermodynamic properties of ABC intercalated alloy with BCC structure at zero pressure. *Journal of Science of HNUE , Natural Sciences*. 2017;62(2): 27-36.
[26] Singh BN, Huang X, Tähtinen S, Moilanen P, Jacquet P, Dekeyser J. *Final report on in-reactor uniaxial tensile deformation of pure iron and Fe-Cr alloy*. Risø National Laboratory Technical University of Denmark Roskilde; 2007.
[27] Isaak DG, Masuda K. Elastic and viscoelastic properties of α iron at high temperatures. *Journal of Geophysical Research: Solid Earth.* 1995;100(B9): 17689-17698.
[28] Adams JJ, Agosta DS, Leisure RG, Ledbetter H. Elastic constants of monocrystal iron from 3 to 500K. *Journal of Applied Physics.* 2006;100(11): 113530.
[29] Sha X, Cohen RE. First-principles thermoelasticity of bcc iron under pressure. *Physical Review*. 2006;B74(21): 214111.
[30] Tang N, Hung VV. Investigation of the thermodynamic properties of anharmonic crystals by the momentum method, (I) General results for FCC crystals. *Phys. Stat. Sol. (b).* 1988;149: 511.
[31] Tang N, Hung VV. Investigation of the thermodynamic properties of anharmonic crystals by the momentum method, (II) Comparison of calculations with experiments for inert gas crystals. *Phys. Stat. Sol. (b).* 1990;161: 165.
[32] Tang N, Hung VV. Investigation of the thermodynamic properties of anharmonic crystals by the momentum method, (III) Thermodynamic properties of the crystals at various pressures. *Phys. Stat. Sol. (b).* 1990;162: 371.

[33] Tang N, Hung VV. Investigation of the thermodynamic properties of anharmonic crystals by the momentum method, (IV) The limiting of absolute stability and the melting temperature of crystals. *Phys. Stat. Sol. (b).* 1990;162: 379.
[34] Magomedov MN. On calculating the Debye temperature and the Gruneisen parameter. *Zhurnal Fizicheskoi Khimii*. 1987;61(4): 1003-1009. (In Russian).
[35] Good RJ, Hope CJ. New Combining Rule for Intermolecular Distances in Intermolecular Potential Functions. *The Journal of Chemical Physics.* 1970;53(2): 540-543.
[36] Magomedov MN. ActivatedProcess Parameters for Diamond, Silicon, and Germanium Crystals. *Russian Microelectronics.* 2011;40(8): 567-573.
[37] O'Sullivan M, Swailes T. A study of historical test data for better informed assessment of wrought iron structures. *International Journal of Architectural Heritage*. 2009;3: 207-215.
[38] *An Introduction to Iron*. Available from: https://www.azom.com/properties.aspx?ArticleID=619 [Accessed 21th October 2020].